Universität Zürich[UZH]

A Test of Lepton Universality in $B^0 \to K^+\pi^-(J/\psi \to \ell^+\ell^-)$ decays

Maximinio Adrover

June 7, 2021

Prof. Nicola Serra
Dr. Patrick Owen
Dr. Rafael Silva Coutinho
Jonas Eschle

Abstract

In light of the recent insight into Lepton Universality violating B-meson decays discovered at the LHCb, a cross-check is performed comparing efficiencies between different B^0 decay modes. In particular the ratio of branching fractions of $B^0 \to K^+\pi^-(J/\Psi \to \ell^+\ell^-)$ with $\ell^\pm = e^\pm, \mu^\pm$ is calculated with the Lepton Universality conforming $B^0 \to K^{*0}(J/\Psi \to \ell^+\ell^-)$ decay as a control channel. Because the lepton pair originates from the J/Ψ the double ratio $R_{J/\Psi}$ should yield unity. The result found in this Thesis of $R_{J\Psi} = 0.982 \pm 0.021$ confirms that the different efficiencies for muon and electron detection remain unchanged for higher hadron invariant masses, and will cancel out in a double ratio of the rare $B^0 \to K^+\pi^-\ell^+\ell^-$ with the resonant J/Ψ-modes.

Contents

1 Introduction

1.1 The Standard Model

During the past century a remarkable shift in our understanding of the universe and the fabric it's made of took place in nearly all disciplines of physics and with it came the advent of particle physics. While it was previously believed that the underlying particles of atoms, namely protons, neutrons and electrons were the basic building blocks of all matter, it was discovered that only the electron could retain its status as a fundamental particle. Both the proton and neutron consist of even tinier constituents, called *quarks*. The electron belongs to its own kind of family of particles, called *leptons*. All quarks and leptons have spin $1/2$, therefore they follow Fermi-Dirac statistics and are referred to as *fermions*, and are structured in three generations. The first generation contains the lightest and most stable particles and the third the most massive ones. Each generation consists of two quarks and two leptons. The species of a particle is commonly referred to as *flavour*, such that there are six quark and three lepton flavours. The first generation contains the *up*- (u) and *down*-quark (d) and the *electron* (e^-) and *electron-neutrino* (ν_e), where the leptons and their corresponding neutrinos share the same flavour. The up-quark carries +2/3 of an electron charge and the down-quarks -1/3. This charge difference between the flavours inside a generation is persistent through all generations and allows the characterization of quarks through their charge as up-type quarks for flavours with charge +2/3 and down-type quarks respectively. Leptons also differ in charge by a single unit in each generation, hence the electron possesses charge -1 while the electron-neutrino is charge neutral. Furthermore, for every fermion there exists a corresponding antiparticle with all the same properties, i.e. equal mass, spin, etc, but with opposite charge. The rest of the particles are listed in Figure 1.
The interactions between those particles are governed by four fundamental forces: the gravitational force, the electromagnetic force, the strong force and the weak force. The behaviour of the above mentioned particles under those forces, where gravity is excluded since its interaction strength all but vanishes at such minute scales, is described by the *Standard Model of Particle Physics* (SM). In this model the interactions between particles are carried out by force carrying particles, called gauge bosons, having integer spin and therefore subject to Bose-Einstein statistics. The electromagnetic force is mediated by the *photon* (γ), the strong force by the *gluon* (g) and the weak force by the W^+, W^- or the Z^0 boson. Lastly the *Higgs* boson (H) endows particles with a mass.

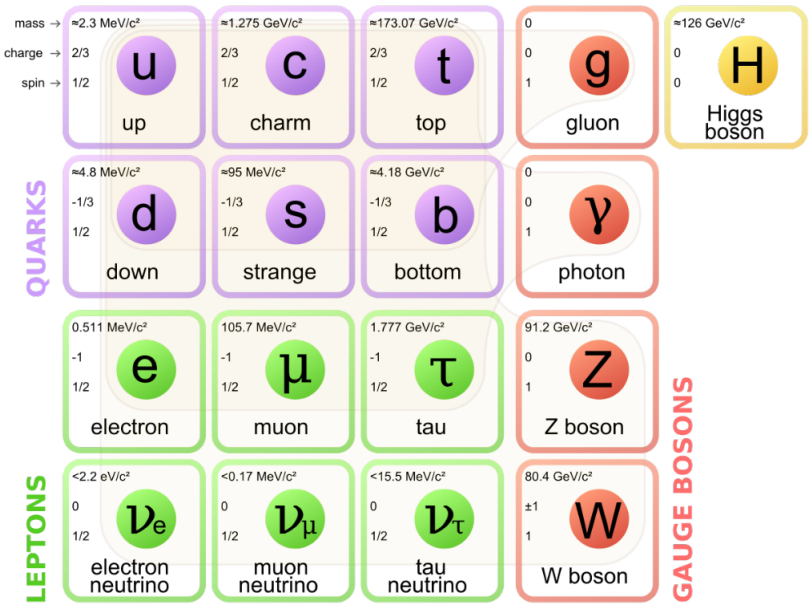

Figure 1: Table of the Elementary Particles

1.2 Lepton Universality and New Physics

The distinguishing property of the $W^{\pm}$ bosons is that they carry a charge of ± 1, while all other gauge bosons are charge neutral. Due to this and charge conservation they can only couple together particles with a difference of one unit of electrical charge. With respect to quarks the 'chargedness' of the W bosons implies that according to the SM a single vertex can only change the flavour of a particle from an up-type to a down-type quark or vice versa. A single interaction involving a Z boson will always leave the flavour unchanged. This is due to the structure of the SM Lagrangian and the unitarity of the Yukawa matrices.
In the SM decays like $B^0 \to K^{*0}\ell^+\ell^-$, where the down-type $\bar{b}$ quark in the B^0 meson ($\bar{b}d$) transitions to another down-type $\bar{s}$ quark (see Figure 2), generally referred to as Flavour Changing Nutral Currents (FCNC), can therefore only occur at higher orders, involving virtual particles and adding vertices to the decay. These are highly suppressed in the SM and therefore such processes lend themselves to searches of physics beyond the SM, often referred to as New Physics (NP).
Moreover the $W^{\pm}$ and Z^0 bosons can couple to any generation of leptons and strong experimental evidence has suggested that they do so independent of flavour, meaning that given a large enough mass they have equal probabilities to decay into an $e^{\pm}$, $\mu^{\pm}$ or $\tau^{\pm}$. This circumstance motivated the statement that the SM exhibits *Lepton Universality* (LU).
Recent and ongoing analyses focusing on B-meson decays of the kind $B \to$

$H\ell^+\ell^-$ through FCNCs, where B denotes a B hadron, i.e. $B^0, B^\pm, \Lambda_b^0$, ..., and H being hadron or a combination of hadrons ($K^\pm, K^{*0}, K\pi$, etc.), found that the ratio of branching fractions

$$R_{K^{*0}} = \frac{\mathfrak{B}(B^0 \to K^{*0}\mu^+\mu^-)}{\mathfrak{B}(B^0 \to K^{*0}e^+e^-)} \tag{1}$$

and

$$R_K = \frac{\mathfrak{B}(B^+ \to K^+\mu^+\mu^-)}{\mathfrak{B}(B^+ \to K^+e^+e^-)} \tag{2}$$

differ from unity significantly, while the SM predicts $R_K \approx 1$ [10]. In both cases the ratio of branching fractions is defined in the dilepton invariant mass-squared range $1.1 < q^2 < 6.0\ GeV^4/c^4$ yielding $R_{K^{*0}}$ = $0.69^{+0.11}_{-0.07} \pm 0.05$ and R_K = $0.846^{+0.042\ +0.013}_{-0.039\ -0.012}$, where the first uncertainty is statistical and the second systematic, with unity being within 2.4-2.5 [1] and 3.1 [4] standard deviations respectively. The analysis of $R_{K^{*0}}$ was published in 2017, whereas the result on the ratio R_K were reported early 2021 further consolidating the evidence of LU violation in these decays. It is suspected that this indicates the existence of an as of yet unknown particle. To claim a discovery however it is generally accepted that the statistical significance of the measurement is no less than five standard deviations, so more measurements are needed.
In order to further solidify the previous results on LU breaking processes, ongoing studies aim to perform a test of lepton universality in other B-meson decay channels, namely $B^0 \to K^+\pi^-\ell\ell$ in the invariant mass region $m_{K^+\pi^-} \in$ [1000 MeV, 2600 MeV]. The goal is to conduct additional measurements with independent systematics and background sources to gather more data and increase the statistical significance.

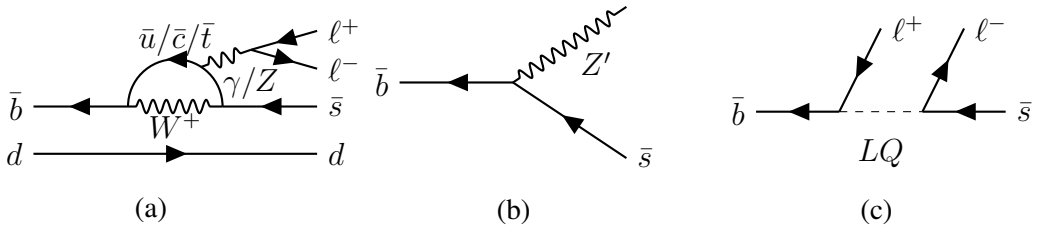

Figure 2: Penguin Diagram of the $B^0 \to K^{*0}\ell^+\ell^-$ FCNC decay (a) and possible NP contributions featuring a hypothetical new boson Z' [8] (b) or a leptoquark [11] (c).

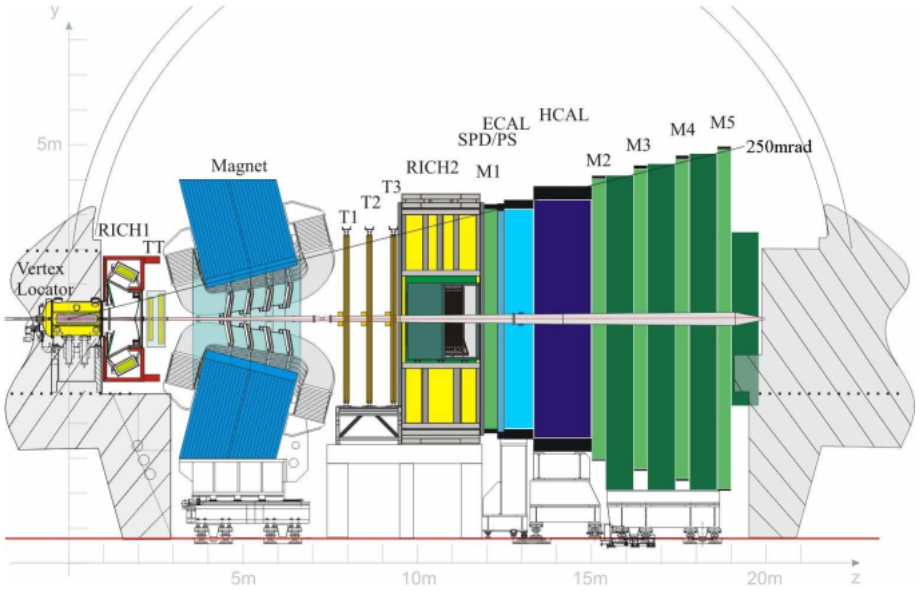

Figure 3: Crosssection of the LHCb Detector [5]

1.3 The LHCb Experiment

The LHCb [5] is one of the four experiments (along with Alice, Atlas and CMS) ongoing at the 27 km long *Large Hadron Collider* (LHC) in Cern, Geneva. It is dedicated to searches of indirect evidence of new physics through studies of CP violation and rare decays of heavy hadrons containing beauty and charm quarks. While the other detectors cover the whole area around the collision points, the LHCb detector is a single-arm spectrometer and has a forward angular coverage from about 10 to 250 mrad in the non-bending plane and operates at a luminosity of about 10^{32} cm^{-2}s^{-1}.

1.3.1 Tracking and Particle Identification

It consists of the *vertex locator* (VELO) located right around the collision point, that provides precise measurements of the primary and secondary vertices (The point in space at which a long lived hadron decays. The displacement between the primary and secondary vertex is a strong signature of b- and c-hadrons.), followed by the first Ring Imaging Cherenkov (RICH) counter that tracks a particle's velocity by measuring the cherenkov emission angle. In order to track a particles trajectory four trackers were put in place. One up- and three in succession downstream of the bending dipole magnet. After the trackers, there is a second RICH module followed by the muon system M1 to M5 and the calorimeters ECAL and

HCAL. The muon system is exclusively dedicated to the detection of muons and the calorimeters measure the transverse energy of particles by completely absorbing them. The momenta from the tracker combined with the velocities determined in the RICH counters allow for precise measurements of the masses of particles passing through and accordingly for particle identification.

1.3.2 Trigger System

Due to the large amount of collisions going on, a fast selection process has to be implemented in order to gather data suitable for analysis. This is achieved via an elaborate trigger system split into the level-0 trigger (L0), implemented at hardware level through custom made electronics, and the high level triggers (HLT) further selecting the data to be stored for analysis.
The L0 trigger operates at a frequency of 40 MHz, which corresponds to the ideal bunch crossing frequency of the LHC, and is designed to reduce the rate of events to approximately 1 MHz. The decision which events to keep are mandated by the high mass of B mesons. Their decay products often exhibit high transverse momentum and energy. It evaluates signals from the VELO, the calorimeters and the muon system only and keeps events that surpass a certain threshold of transverse energy and momentum.
The HTL consists of two stages, HLT 1 and HLT 2, both implemented in software, running centrally on a computing farm close to the detector [2]. It has access to all information gathered by the various parts of the detector and aims to fully reconstruct events, reducing the rate of collisions saved for analysis to 12.5 kHz.

1.4 The J/ψ Decay Mode

For a number of reasons the efficiency of the detector towards detecting electrons is quite different compared to its muon detection efficiency, with the latter exhibiting an overall much cleaner signature and therefore higher efficiency. This is partly due to the lower acceptance at the L0 trigger, requiring a transverse momentum of $p_T^e \sim 2.4$ GeV for electrons and $p_T^\mu \sim 1.8$ GeV for muons [2], and the fact that electrons emit higher amounts of bremsstrahlung possibly leading to less energy deposited in the ECAL, if not properly accounted for. This leads to a reconstruction efficiency for muonic decays that is about five times larger than for electronic decays [1].
In order to avoid an in-depth analysis of the efficiencies the resonant $B^0 \to K^{*0}(J/\psi \to \ell^+\ell^-)$ decay might be used as a control channel by calculating the

double ratio

$$R_{K\pi} = \frac{\mathfrak{B}(B^0 \to K^+\pi^-\mu^+\mu^-)}{\mathfrak{B}(B^0 \to K^+\pi^-e^+e^-)} \Bigg/ \frac{\mathfrak{B}(B^0 \to K^{*0}(J/\psi \to \mu^+\mu^-))}{\mathfrak{B}(B^0 \to K^{*0}(J/\psi \to e^+e^-))}. \quad (3)$$

This method is particularly useful because the branching fractions are proportional to their corresponding event yields divided by the detector efficiency. In calculating the double ratio the efficiencies and proportionality constants cancel out individually and no contribution comes from the control channels, since the decay $J/\Psi \to \ell^+\ell^-$ is known to be consistent with LU [9]. Because of its very narrow width the J/ψ lends itself as a control channel. Decays, involving the charmonium, occur at tree-level, as depicted in fig. 4, and are therefore not naturally suppressed and have branching fractions about four orders of magnitude larger than the $B^0 \to K^+\pi^-\ell^+\ell^-$ mode [9].
This thesis aims to provide a crosscheck that the relative efficiencies cancel as well between the non-resonant $B^0 \to K^+\pi^-(J/\psi \to \ell^+\ell^-)$ and the resonant $B^0 \to K^{*0}(J/\psi \to \ell^+\ell^-)$ modes. The efficiencies are confirmed to cancel out between the resonant and non-resonant mode, if the following ratio

$$R_{J/\Psi} = \frac{N(B^0 \to K^+\pi^-(J/\psi \to \mu^+\mu^-))}{N(B^0 \to K^+\pi^-(J/\psi \to e^+e^-))} \Bigg/ \frac{N(B^0 \to K^{*0}(J/\psi \to \mu^+\mu^-))}{N(B^0 \to K^{*0}(J/\psi \to e^+e^-))} \quad (4)$$

yields unity. Where N represents the number of events measured of a given decay.

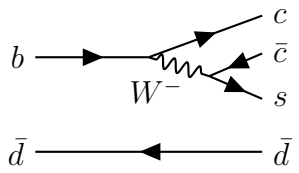

Figure 4: The decay subject to this analysis: $B^0 \to k^{*0}(J/\psi \to \ell^+\ell^-)$

In order to extract the yields of the individual decay channels a fit was applied to the four body invariant mass of the B^0 decay. In a first step the parameters of the Probability Density Function (PDF) of the signal (Section 3.1) were determined via simulated data samples (Section 3.2). The different background sources described in Section 2.2 and signal were modeled separately such that only events associated with the decay of interest contribute to the yield (Section 3.3), fixing the parameters to the values of the Monte Carlo fit, such that only mean and width of the PDFs modelling the signals are able to vary freely. In a final step the extracted yields were plugged into equation 4 to compute the ratio with its associated error (Section 4).

2 Data and Background-Selection

The data subject to this analysis was gathered during run 2 of the LHC in 2016 at a centre of mass energy of $\sqrt{s} = 13$ GeV and corresponds to an integrated luminosity of 1.643 fb^{-1} for events where the B^0 decays into muons and 1.645 fb^{-1} for electrons respectively. A kinematic fit was applied, requiring the decay products to originate from the same primary vertex, and in calculating the mass of the B^0, the dilepton mass was fixed to the J/ψ, which vastly improves resolution because it mitigates adverse effects like energy loss of leptons due to bremsstrahlung.

2.1 Monte Carlo Simulation

In addition to the data gathered from directly detecting proton-proton (pp) interactions, an in-depth analysis requires samples generated through simulations, often referred to as Monte Carlo (MC) Data. It is treated in a very similar way as the real data would. The main difference being that the pp-interactions as well as the detector and L0-trigger response are simulated by a set of specialized applications [6]. The reconstruction and stripping of the simulated samples is handled by the HLT on the processing farm as is the corresponding data, gathered from real interactions. This is done to optimize data acquisition and to better understand potential background sources.
In this thesis the MC data was used to fix some of the parameters of the fit, as seen in Section 3.

2.2 Selections and Residual Background

In order to compare the resonant mode to the non resonant modes the B^0 mass was evaluated in three regions for electrons and muons respectively. First the resonant mode, where the Kπ-mass corresponds to the mass of the $K^{*0}(892)$, was selected in the range

$$m_{K\pi} \in [795.9 \text{ MeV}, 995.9 \text{ MeV}].$$

The non resonant mode was split into two parts, due to a background signal originating from a D-meson (containing a charm quark) decay as depicted in Figure 5. To reject the signal, hadron pairs with masses between 1835 and 1895 MeV were dismissed, leaving the two regions

$$m_{K\pi} \in [1000 \text{ MeV}, 1835 \text{ MeV}]$$

and

$$m_{K\pi} \in [1895 \text{ MeV}, 2600 \text{ MeV}]$$

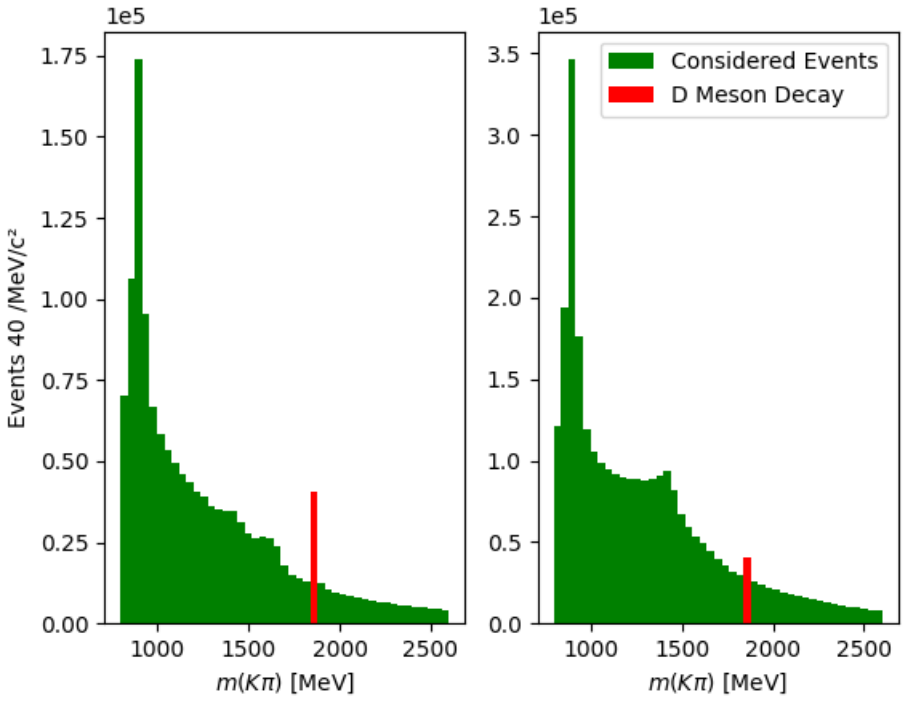

Figure 5: Invariant Hadron masses measured for electrons (left) and muons (right)

for evaluation.
The distinction between signal and background was performed via a multi variate analysis using XGBoost [3], a scalable tree boosting system. It assigns each event a label score between zero and one, where the likelihood of an event to be signal is expected to be higher, the closer to one the label score is. For this analysis the XGB Label score χ for each event is required to satisfy $\chi > 0.999$.
In addition to the J/ψ restriction mentioned above the q^2 variable of the Ntuples were required to be in the region

$$7 < q^2 < 11\ GeV^2/c^4.$$

2.2.1 Partially Reconstructed Background

In reconstructing the B meson, in a large portion of the events one or more of the decay products evade detection. This leads to events exhibiting a lower mass than is to be expected. In Figure 6 it is visible as the shoulder before the peak at the B^0 mass $m_{B^0} \approx 5280$ MeV.

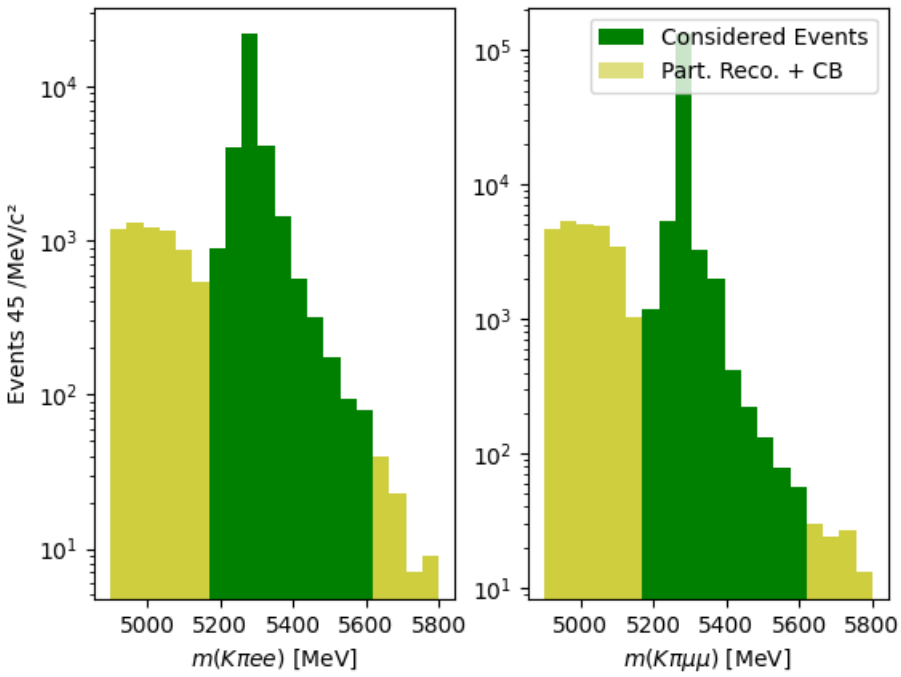

Figure 6: Reconstructed invariant mass of the four body decay: The shoulder colored yellow in the lower mass region can be accounted to partially reconstructed background. The tail in the higher mass region is mostly due to combinatorial background. Only events within the [5150, 5600 MeV] window were considered.

In order to improve the quality of the fit, this part of the data was cut out of the sample. Only events with a mass larger than 5150 MeV were considered.

2.2.2 Combinatorial Background

A common problem in particle physics is the multitude of decay products originating from a single pp-interaction and that the assignment of particles to a specific decay is not apparent. It is impossible to tell which particles originated from the same decay and in general there are more possible combinations of particles than decays from which they stem from. This leads to an additional source of background, usually referred to as Combinatorial Background (CB), which needs to be accounted for. The CB exhibits exponential behaviour, decreasing as the energy increases, therefore it can be approximated by an exponential function as described in Section 3.
At 5600 MeV the peak of the B^0 is sufficiently far away to assume that everything

beyond can be accounted to CB. Therefore only events with $m_{B^0} < 5600$ MeV were considered in this analysis.

2.2.3 Background from Suppressed B_s Decays

In Figures 9 and 10 a significantly smaller peak is visible at approximately 5360 MeV. It is due to a B_s^0 ($s\bar{b}$) meson decaying into the same decay products as the B^0 in a similar fashion as the D^0 from Section 2.2. It is however treated differently to the background from D^0 mesons because its mass is much closer to the desired 5280 MeV. Instead of dismissing the signal altogether it was considered in the fit and subsequently subtracted from the signal yield (Sections 3. and 4.).

2.2.4 Particle Miss-Identification

Using the information from the individual parts of the detector, particles triggering an event are assigned a mass hypothesis, depending on the signature they leave. In some cases however particles are misidentified and are assigned an erroneous mass hypothesis. In reconstructing the decaying particle this leads to a shift in the invariant mass to higher values if the mass hypothesis is larger than the actual mass of the detected particle and vice versa. An example of such a case is depicted in Figure 7. The apparent signal resulting from misidentification greatly decreases the quality of the fit. To mitigate its effects, a cut was applied removing all entries where the reconstructed mass of the B meson, replacing the kaon-mass with the pion-mass, lies within [5300 MeV, 5450 MeV]. This approach is justified by the fact that firstly we are not interested in the $B_s^0 \to \pi^+\pi^-(J/\psi \to \ell^+\ell^-)$ decay, and secondly the amount of events due to this decay is negligible compared to the signal

3 Fitting Method

In order to extract the signal yields an extended unbinned negative log-likelihood fit was applied to the invariant mass $m(K^+\pi^-\ell^+\ell^-)$ of the four-body decay. For both the muon and electron channel the fit was performed over an invariant mass range from 5150 MeV to 5600 MeV. The parameters of the probability density functions (PDFs) for the signals are determined from MC data and only the mean and width are allowed to vary in the fit to the data.

3.1 Probability Density Functions

The fit consists of the sum of three seperate PDFs modelling the signal itself, the signal due to the B_s^0 and the combinatorial background. Both signals were

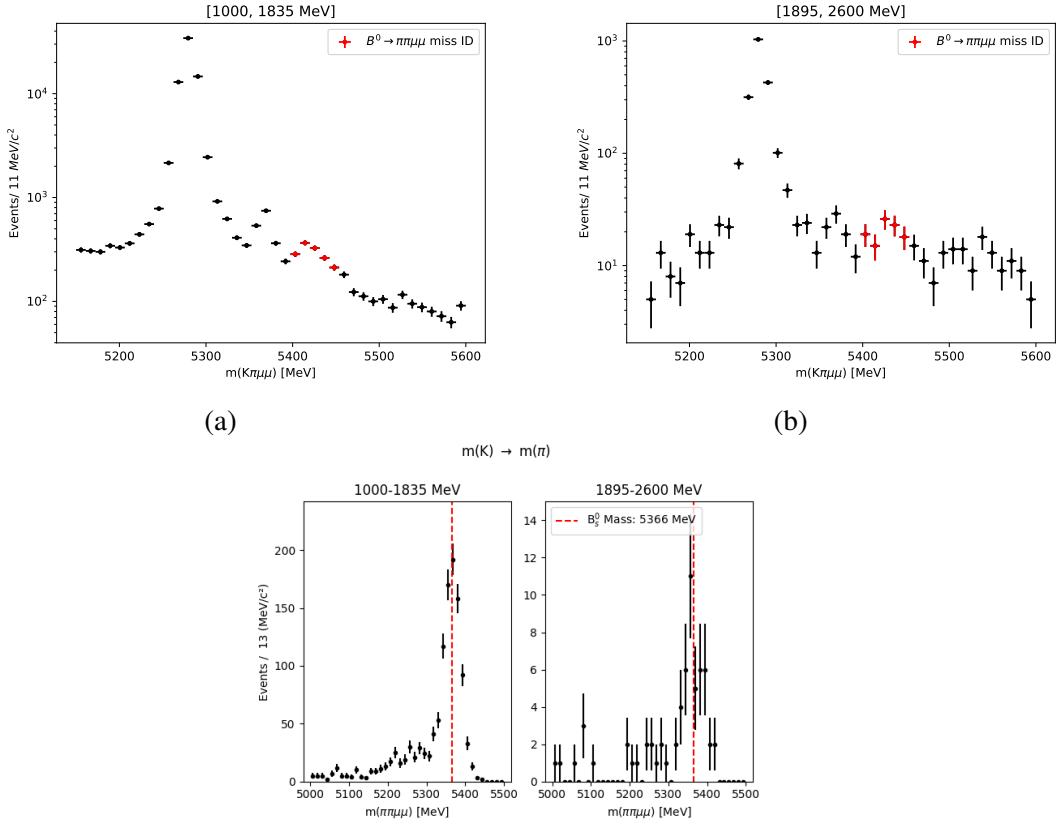

Figure 7: The histograms (a) and (b) exhibit a third slightly smaller peak at about 5440 MeV that is due to particle miss identification. It stems from a B_s^0 decaying into two pions, where one of them was misidentified as a kaon. This becomes apparent when the events between 5400 and 5450 MeV are reconstructed switching the mass of the kaon to that of a pion as is done in figure (c). A peak is visible at about 5366 MeV which corresponds to the mass of the B_s^0.

modelled by a Double Sided Crystal Ball (DSCB) function. The Crystal Ball function, named after the Crystall Ball Collaboration by whom it was developed [12], is a C^1-function, consisting of a central gaussian function with a power law tail.

$$f(x;\alpha,n,\mu,\sigma) = \begin{cases} e^{-\frac{1}{2}(\frac{x-\mu}{\sigma})^2} & , \frac{x-\mu}{\sigma} > -\alpha \\ (\frac{n}{|\alpha|})^n e^{\frac{1}{2}|\alpha|^2} (\frac{n}{|\alpha|} - |\alpha| - \frac{x-\mu}{\sigma})^{-n} & , \frac{x-\mu}{\sigma} < -\alpha \end{cases} \tag{5}$$

The parameters μ and σ describe mean and width of the Gaussian core, while

α and n give the value at which the power law tail crosses over to the gaussian section of the curve, and the slope of the power law. In a Double Sided Crystal Ball function both tails are described by a power law, adding two more parameters α_R and n_R (whereas α and n will be labeled α_L and n_L) to a total of six parameters.
This function is typically used in high energy physics to model loss afflicted processes such as the reconstruction of invariant masses from energies and four-momenta of decay products. The combinatorial background is modelled by an exponential function. The single parameter is free to vary in the fit.

3.2 Fits to the Monte Carlo Simulation

The fits are applied using the zfit package [7]. The MC data reproduces the resonant mode of the decay subject to this analysis, that is $\mathrm{B}^0 \to K^*(892)(J/\psi \to \ell^+\ell^-)$. Listed below are the parameters that best fit the simulated data:

	e^+e^-	$\mu^+\mu^-$
μ	5281 MeV	5280 MeV
σ	9.571 MeV	6.816 MeV
α_L	0.734	1.249
n_L	2.592	2.238
α_R	0.707	1.294
n_R	2.116	2.501

Table 1: Parameters of the fit to the MC data for the electron and muon channel. The errors on the parameters are disregarded here because they have no influence on the resulting errors on the yields

The quality of the fit can be improved by adding a gaussian distribution to the model sharing the same mean and width as the DSCB.

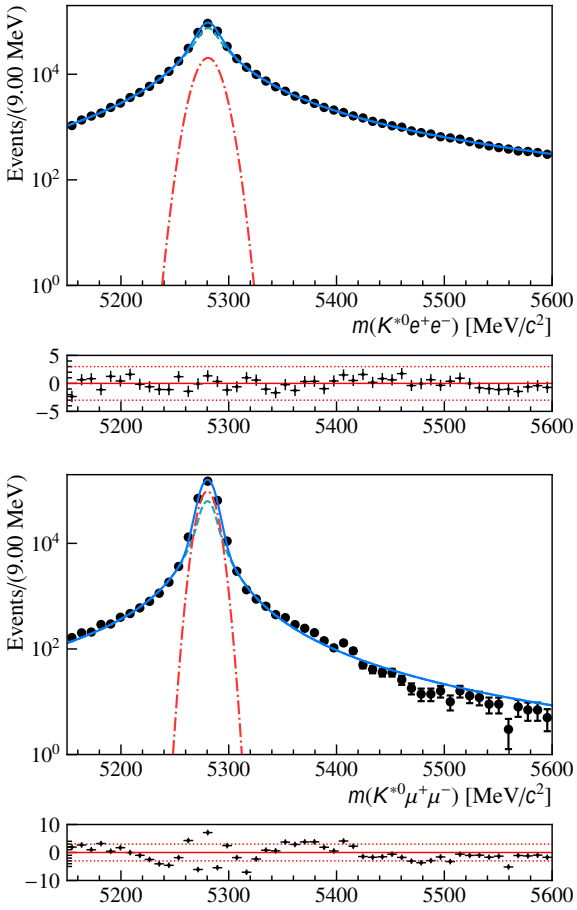

Figure 8: Mass fits to the MC simulated resonant decay modes. The signals were fitted with a double sided crystal ball function (dashed light blue) and a gaussian function (dotted dashed red) sharing mean and width. The sum of both PDFs is depicted by a solid dark blue line.

3.3 Fits to the Data

Each PDF was assigned an additional parameter, namely the yield, associating each one with the number of events related to the PDFs. This allows for enumerating the events responsible for the signal of interest, physical background signal, and combinatorial background respectively.
Because of the less stable nature of the actual data compared to the MC samples some adjustments had to be made to the fitting method, especially the electron channel, due to its overall worse signature.

3.3.1 Electron Channel

In a first step the additional gaussian contribution to the signal was dropped, while keeping the parameters of the MC fit unchanged. Because the background signal nearly vanishes in the slope of the main signal, the following parameters were fixed in their respective $m_{K\pi}$ regions for optimal fit fidelity:

- 795.9 MeV $< m_{K\pi} <$ 995.9 MeV:
  - The mean of the signal μ was fixed to μ = 5280 MeV.
  - The mean of the background signal $\mu_{B_s^0}$ was fixed to the PDG value $\mu_{B_s^0}$ = 5366 MeV [9].
  - The width of the background signal $\sigma_{B_s^0}$ was fixed to the value found in the muon channel resonant mode $\sigma_{B_s^0}$ = 8.632 MeV.
- 1000 MeV $< m_{K\pi} <$ 1835 MeV:
  - The mean of the background signal $\mu_{B_s^0}$ was fixed to the PDG value $\mu_{B_s^0}$ = 5366 MeV.
- 1895 MeV $< m_{K\pi} <$ 2600 MeV:
  - The background signal was disregarded because no distinction is possible between CB and the B_s^0-signal.

As in the MC-fit the signal due to the B_s^0 was modelled with a DSCB with an additional gauss distribution.

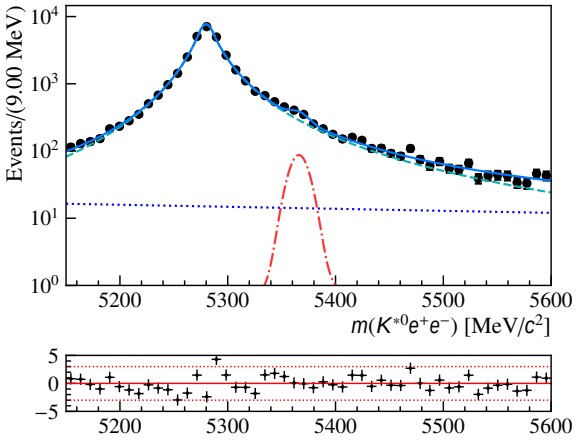

(a)

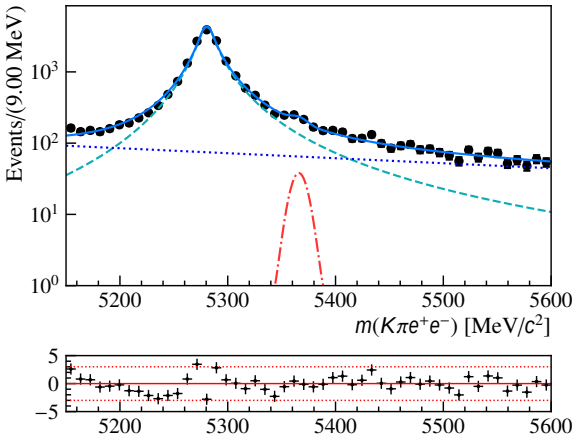

(b)

Figure 9: Mass fits to the $B^0 \to K\pi(J/\psi \to e^+e^-)$ channel in the resonant mode $m(K\pi) \in$ [795.9, 995.9 MeV] (a) and the lower non-resonant mode $m(K\pi) \in$ [1000 ,1835 MeV] (b). The dashed light blue line is the fit associated to the signal yield. The dotted dashed red line models the B_s^0 mass and the dotted dark blue line the CB. The solid dark blue line represents the sum of the PDFs.

3.3.2 Muon Channel

Less adjustments were necessary for the muon channel. In fact only the mean of the background signal $\mu_{B_s^0}$ was fixed to the PDG value. Otherwise all parameters were able to vary freely except the ones fixed to the MC-fit values.

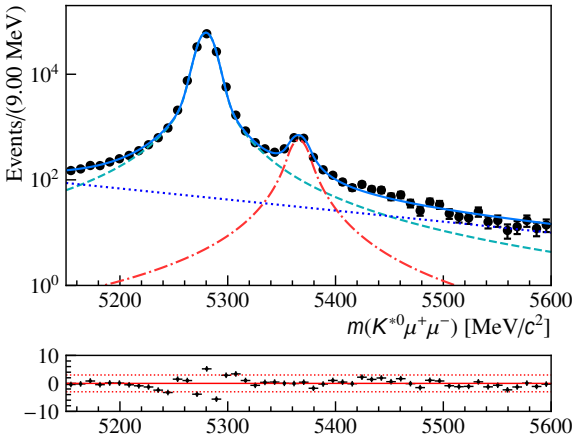

(a)

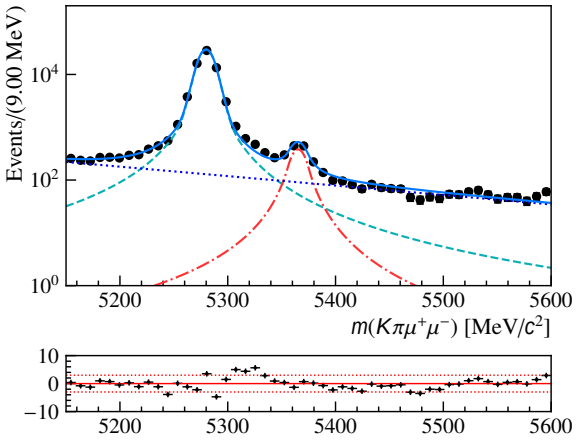

(b)

Figure 10: Mass fits to the $B^0 \to K\pi(J/\psi \to \mu^+\mu^-)$ channel in the resonant mode $m(K\pi) \in$ [795.9, 995.9 MeV] (a) and the lower non-resonant mode $m(K\pi) \in$ [1000 ,1835 MeV] (b). The dashed light blue line is the fit associated to the signal yield. The dotted dashed red line models the B_s^0 mass and the dotted dark blue line the CB. The solid dark blue line represents the sum of the PDFs.

The mass fits to the non-resonant decay in the higher $m(K\pi) \in$ [1895, 2600 MeV] region were also considered and can be found in the appendix A.

4 Yields and Result

Listed below are the signal yields of the individual fits:

$m(K\pi)$ [MeV]	795.9 - 995.9	1000 - 1835	1895 - 2600
e^+e^-	34750 $\pm$ 230	17420 $\pm$ 170	476 $^{+29}_{-28}$
$\mu^+\mu^-$	140700 $\pm$ 380	69160 $\pm$ 270	2019 $^{+48}_{-47}$

Table 2: Signal yields of the different channels for the individual $m(K\pi)$-regions. For the high Kπ-mass region the errors are given as the upper and lower boundary.

The ratio $R_{J/\Psi}$ in Equation 4 is calculated, where the entries of the first column of Table 4 correspond to the respective $N(B^0 \to K^{*0}(J/\psi \to \ell^+\ell^-))$ and $N(B^0 \to K^+\pi^-(J/\psi \to \ell^+\ell^-))$ is given by the sum of the entries of the lower and higher $m(K\pi)$ regions.

$$R_{J/\Psi} = 0.982 \pm 0.021$$

The errors on the ratio were determined with guassian error propagation on the upper and lower bounds individually. The upper and lower bounds are identical up to significant digits, so they are summarized in the result.

5 Conclusion

The result on the ratio $R_{J/\Psi}$ is in very good agreement with unity and confirms that the relative efficiencies remain unchanged between the resonant and non-resonant mode. It indicates that in ongoing tests of lepton universality of the $B^0 \to K\pi\ell\ell$ decays, the resonant mode including the J/Ψ can be used as a control channel, as in the double ratio defined in Equation 3. The statistics available for the K^{*0} modes are superior compared to the non-resonant modes. This circumstance manifests itself in table 4, where the signal yield of the resonant mode is approximately twice as large as the yields of the higher $K\pi$-mass regions, and promises to facilitate ongoing analyses.

Further effort could be put into the identification of individual background sources. For instance, there were no measures taken in this analysis to extract events resulting from miss-IDs where one of the kaons originating from a $B_s^0 \to K^+K^-(J/\Psi \to \ell^+\ell^-)$ was misidentified as a pion. These events would populate the signal region and might influence the signal yield to a slight degree.

By taking more of such processes into account, the error on the double ratio could be reduced by some amount. But since the result is very close to the expected value, the implication on further proceedings in LU tests will remain the same.

Appendix

A 1895 MeV $< m(K\pi) <$ 2600 MeV

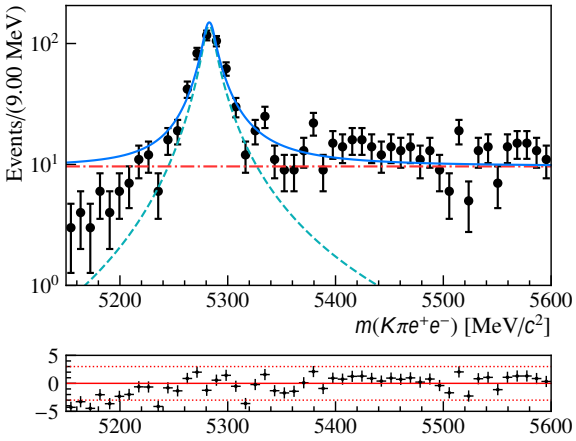

Figure 11: Mass fit to the higher non-resonant mode. The light blue dashed line is the fit associated to the signal. The dotted dashed red line fits the CB and the solid blue line represents the sum of the PDFs. Due to bad convergence, the B_s^0 mass was not modeled here.

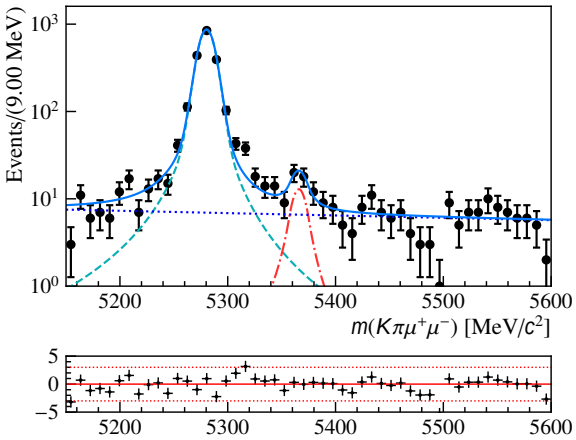

Figure 12: Mass fit to the higher non-resonant mode. The light blue dashed line is the fit associated to the signal. The dotted dashed red line models the B_s^0 mass and the dotted dark blue line the CB. The solid blue line represents the sum of the PDFs. The drop in events around 5500 MeV is likely due to the cut on miss identified pions as described in Section 2.2.4.

References

[1] R. Aaij et al. "Test of lepton universality with $B^0 \to K^{*0}\ \ell^+\ell^-$ decays". In: *Journal of High Energy Physics* 2017.8 (Aug. 2017). ISSN: 1029-8479. DOI: 10.1007/jhep08(2017)055. URL: http://dx.doi.org/10.1007/JHEP08(2017)055.

[2] Roel Aaij et al. "Design and performance of the LHCb trigger and full real-time reconstruction in Run 2 of the LHC." In: *JINST* 14.arXiv:1812.10790. 04 (Dec. 2018), P04013. 43 p. DOI: 10.1088/1748-0221/14/04/P04013. URL: https://cds.cern.ch/record/2652801.

[3] Tianqi Chen and Carlos Guestrin. "XGBoost". In: *Proceedings of the 22nd ACM SIGKDD International Conference on Knowledge Discovery and Data Mining* (Aug. 2016). DOI: 10.1145/2939672.2939785. URL: http://dx.doi.org/10.1145/2939672.2939785.

[4] LHCb collaboration et al. "Test of lepton universality in beauty-quark decays". In: (2021). arXiv: 2103.11769 [hep-ex].

[5] The LHCb Collaboration et al. "The LHCb Detector at the LHC". In: *Journal of Instrumentation* 3.08 (Aug. 2008), S08005–S08005. DOI: 10.1088/1748-0221/3/08/s08005. URL: https://doi.org/10.1088/1748-0221/3/08/s08005.

[6] G Corti et al. "How the Monte Carlo production of a wide variety of different samples is centrally handled in the LHCb experiment". In: *J. Phys.: Conf. Ser.* 664.LHCb-PROC-2015-016. CERN-LHCb-PROC-2015-016. 7 (May 2015), 072014. 8 p. DOI: 10.1088/1742-6596/664/7/072014. URL: https://cds.cern.ch/record/2019805.

[7] Jonas Eschle et al. "zfit: Scalable pythonic fitting". In: *SoftwareX* 11 (Jan. 2020), p. 100508. ISSN: 2352-7110. DOI: 10.1016/j.softx.2020.100508. URL: http://dx.doi.org/10.1016/j.softx.2020.100508.

[8] Rhorry Gauld, Florian Goertz, and Ulrich Haisch. "An explicit Z-boson explanation of the B $\to$ K$^{\mu^+\mu^-}$ anomaly". In: *Journal of High Energy Physics* 2014.1 (Jan. 2014). ISSN: 1029-8479. DOI: 10.1007/jhep01(2014)069. URL: http://dx.doi.org/10.1007/JHEP01(2014)069.

[9] Particle Data Group et al. "Review of Particle Physics". In: *Progress of Theoretical and Experimental Physics* 2020.8 (Aug. 2020). 083C01. ISSN: 2050-3911. DOI: 10.1093/ptep/ptaa104. eprint: https://academic.oup.com/ptep/article-pdf/2020/8/083C01/34673722/

ptaa104.pdf. URL: https://doi.org/10.1093/ptep/ptaa104.

[10] Gudrun Hiller and Frank Krüger. "More model-independent analysis of $\vec{b}\ s$ processes". In: *Phys. Rev. D* 69 (7 Apr. 2004), p. 074020. DOI: 10.1103/PhysRevD.69.074020. URL: https://link.aps.org/doi/10.1103/PhysRevD.69.074020.

[11] Jogesh C. Pati and Abdus Salam. "Lepton Number as the Fourth Color". In: *Phys. Rev. D* 10 (1974). [Erratum: Phys.Rev.D 11, 703–703 (1975)], pp. 275–289. DOI: 10.1103/PhysRevD.10.275.

[12] Tomasz Skwarnicki. "A study of the radiative CASCADE transitions between the Upsilon-Prime and Upsilon resonances". PhD thesis. Cracow, INP, 1986.